Characterization of gain and directivity of exponential horn receivers[a)]

Daniel J. Mennitt[b)]
Department of Electrical and Computer Engineering, Colorado State University, 1373 Campus Delivery, Fort Collins, Colorado 80525, USA

Kurt M. Fristrup
Natural Sounds and Night Skies Division, National Park Service, 1201 Oakridge Drive, Fort Collins, Colorado 80525, USA

Branislav M. Notaros
Department of Electrical and Computer Engineering, Colorado State University, 1373 Campus Delivery, Fort Collins, Colorado 80525, USA

(Received 4 April 2017; revised 30 September 2017; accepted 7 November 2017; published online 27 November 2017)

It is difficult and expensive to match the sensitivity of the most sensitive vertebrate ears with off-the-shelf microphones due to the self-noise of the sensor. The extremely small apertures of micro-electromechanical microphones create options to use horn waveguides to amplify sound prior to transduction without resulting in an unacceptably narrow directivity. Substantial gain can be achieved at wavelengths larger than the horn. An analytical model of an exponential horn embedded in a rigid spherical housing was formulated to describe the gain relative to a free-field receiver as a function of frequency and angle of arrival. For waves incident on-axis, the analytical model provided an accurate estimate of gain at high frequencies as validated by experimental measurement. Numerical models, using the equivalent source method, can account for higher order modes and comprehensively describe the acoustic scattering within and around the horn for waves arriving from any direction. Results show the directivity of horn receivers were adequately described by the analytical model up to a critical wavelength, and the mechanisms of deviation in gain at high frequencies and large angles of arrival were identified.
https://doi.org/10.1121/1.5012757

[JFL] Pages: 3257–3266

I. INTRODUCTION

Autonomous recording technology is increasingly applied to efficiently monitor wildlife behavior[1] and abundance.[2] Animal presence is often more easily heard than seen[3] and passive monitoring of sound is a noninvasive alternative to visual observations or physical capture.[4] Passive acoustic monitoring can also provide information on physiographic conditions, human activity, and noise pollution on a wide range of spatial and temporal scales.[5] Microphone self-noise is the primary limiting factor for this technology; it compromises the spatial coverage of the instruments and the signal-to-noise ratios of the recordings.

Sensitive microphones are also essential to document the adventitious sounds of nature and the degree to which noise pollution degrades wildlife awareness of these sounds. Noise pollution is pervasive, extending beyond urban areas and transportation corridors into many rural and protected areas such as United States National Parks.[6] The behavior and health of humans, as well as non-human animals, is affected by the sounds of their surroundings; the increase of environmental noise levels worldwide has motivated research on the effects of noise on humans[7] and wildlife.[8]

This paper analyzes horns as receivers to introduce gain and control directivity for passive acoustical monitoring in terrestrial environments. Acoustical measurements are a primary data source for the methods of noise control, acoustic ecology,[9] bioacoustics, and other disciplines. Most measurements could be broadly lumped into two categories: encompassing all sources over a large area (environmental monitoring) and directed at a single acoustic source or direction (focused measurements). Environmental monitoring requires receivers with omnidirectional sensitivity for both coverage and calibration whereas focused measurements can benefit from unidirectional sensitivity. Because natural sounds are often significantly quieter than human caused noise, measurements in both categories can be limited by the noise-floor of recording equipment.

The instruments developed to address urban noise problems present some significant limitations for environmental monitoring in very quiet areas, remote settings, and studies requiring dense sampling. For example, the Unites States National Park Service uses type-1 sound level meters for measurements of acoustical resource conditions, which have a direct implication to visitor experience and wildlife fitness. The self-noise,[10] cost, and power consumption, and limited

[a)]Portions of this work were presented in "Gain and directivity of exponential horn receivers," J. Acoust. Soc. Am. **140**, 3140 (2016).
[b)]Electronic mail: dmennitt@rams.colostate.edu

data storage of precision sound level meters constrain the scope of their application, though they serve as valuable reference instruments. Figure 1 shows one-third octave band L_{90} sound pressure levels from 491 seasonally-averaged observations at sites located in diverse acoustical environments throughout the United States. Environmental sound levels often exhibit a $1/f$ power spectrum and therefore lower levels at higher frequencies.[11] Because natural acoustical conditions are quiet relative to urban areas, the self-noise of the sound level meter exceeds that of the acoustical environment in the upper one-third octave bands. Each concentration of traces in Fig. 1 indicates the self-noise of a particular generation of equipment and device configuration over years of monitoring. Although Fig. 1 shows daytime levels, nighttime levels are often quieter and therefore more difficult to measure. From a resource protection standpoint, the inadequacy of available hardware results in the inability to document existing conditions in the quietest places and quantify the extent to which polluted areas have been degraded.

Focused measurements typically target a single vocalizing animal or area, such as that in the field of view of a camera trap. Most work in the field of bioacoustics has studied intentional vocalizations; however, animals also produce and respond to incidental sounds such as movement. These sounds are typically much quieter than intentional vocalizations and efforts thus far have been limited to on-animal recordings and large animals.[12] However, incidental sounds are critical to many predator-prey interactions and can offer valuable information about physiological, behavioral, and ecological processes. For example, some gleaning bats hunt by passively listening for subtle sounds produced by the movement of insects.[13] Remote measurement of incidental sounds requires extremely sensitive measurements. In fact, the amplitude and characteristics of these incidental sounds are largely unknown because the self-noise of available equipment limits our ability to measure them. However,

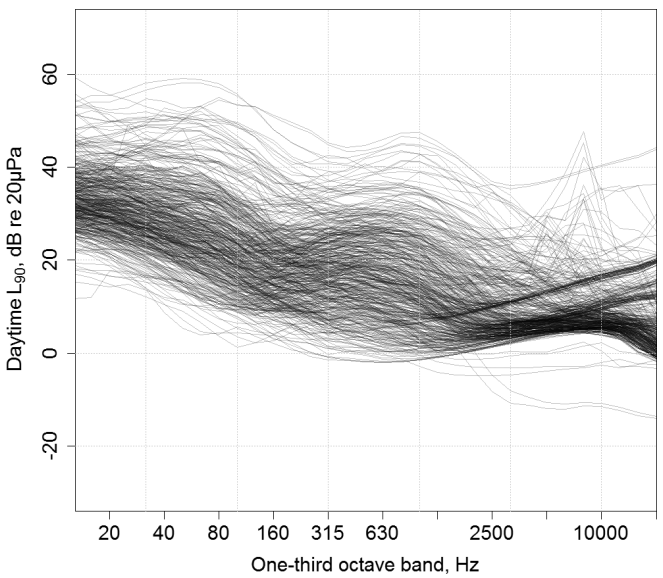

FIG. 1. 491 seasonal observations of background sound levels (L_{90} dB sound pressure level) from type-1 measurements in US national parks.

invertebrate audiograms show that some animals have hearing more sensitive than the quietest available microphones[14] and the evolutionary investment in this ability strongly suggests that there is information worth sensing. The study of animal behavior, and especially bioacoustic interactions involving incidental sounds, can benefit from the ability to measure the very quiet signals that the animals themselves can hear and produce.

The measurement of extraordinary phenomena requires extraordinary tools. There are several strategies that can increase the effectiveness of a receiver system including microphone arrays, parabolic reflectors, and horns. Measurement systems designed to acquire acoustical data commonly consist of a microphone, signal conditioning, audio-digital conversion, and storage of data. While all of these components can contribute noise, the microphone is often the limiting factor. Fundamentally, the voltage output from a microphone is proportional to the area of the diaphragm. However, the larger the diaphragm the greater the reduction in high frequency response as wavelength becomes comparable to diaphragm diameter. Additionally, the stiffness will decrease and the increased inertia makes it slow to respond to high frequency sound. Arrays are typically constructed for localization and beamforming. Coherent measurements from an array of multiple microphones can also provide gain relative to incoherent sensor noise at a rate of 3 dB per doubling of elements. Theoretically, adequate measurements are possible with a copious number of sensors, but the cost and complexity of hardware and array processing makes this approach practically prohibitive in applications requiring high gain or dense spatial sampling. Another class of approaches is to amplify the acoustic energy before it reaches the microphone, as in parabolic dishes and horns. The geometry of a parabolic dish is such that it focuses sound on a microphone oriented at the focal point of a dish. A microphone securely orientated at the focal point of a parabolic dish will receive multiple coherent reflections of a wave incident on the dish area. If large, parabolic dishes can provide high gain and have been effective in focused monitoring that target a single source (e.g., wildlife studies) and therefore benefit from high directivity.[15] However, environmental monitoring requires uniform directivity as discussed above. We find horns to have significant advantages for acoustic monitoring that requires measurements with low-self noise, low power, portability, low cost, and control of directivity. Whereas the gain of most acoustic devices is proportional to area, the gain of a horn is proportional to the ratio of the mouth to throat areas. Therefore, a horn can produce more gain than a parabolic dish of equivalent size, as well as allowing for control of directivity.

The horn is a waveguide with cross sectional area that increases along its length from the throat to the mouth. A horn increases the radiation efficiency of an acoustic source positioned at the throat and affects the directivity of radiated sound. The horn is a fundamental acoustic device, with widespread use throughout human history as well as by non-human animals.[16] Today, horns are primarily used for transmission of sound in applications such as public address systems, sound reinforcement systems, and musical

instruments. Alternatively, horns can be used as a receiver in which sound is incident on the mouth and travels to a microphone located at the throat. The horn acts like a hydraulic press that multiplies force over a change in area; to a first order approximation, the gain provided is proportional to the ratio of the mouth to throat area.

Historically in the early age of microphone technology, the horn as a receiver had been considered to overcome the self-noise of the microphone and amplifier.[17] While this mode of operation persists in biological systems, with few exceptions[18] the horn as a receiver has fallen out of interest because advancements in electrical technology have made equipment that is suitable for most applications widely available. Furthermore, given the size of conventional microphone diaphragms, horns must be very large to achieve any benefit. In addition to the logistical difficulties, a large receiver is acoustically very directive. Considering the objectives of environmental monitoring, very small transducers are required to make horn receiver systems feasible. In the past few decades, micro-electro-mechanical technology has matured to the point where very small, well-performing, microphones are widely available and cost-effective. The potential for further increases in performance rises with progressively smaller transducers.[19]

In this paper, we analyze the horn as an acoustic pressure receiver in which the geometry can be designed to control the directivity and frequency response of acoustical measurements. The study of horn theory and the one-dimensional approximation known as Webster's horn equation has a long history.[20] Here, we incorporate this approximation into a direction-dependent analytical model to analyze the horn as a receiver of far-field acoustic waves. Using numerical models, we show the applicability of the analytical approach as it applies to direction, frequency, and horn geometry. While the limitations of Webster's approximation have been shown for transmission,[21] the characteristics of the horn as a receiver is less well known. Studies have investigated the relative utility of an analytical approximation and numerical method to describe the internal sound field of the human ear canal.[22] Here, we examine the case of an exponential horn embedded in a rigid spherical housing for its generality. A spherical housing also possesses excellent diffraction characteristics considering the omnidirectional requirement of environmental sound monitoring. Section II details the analytical, experimental, and numerical methods used to analyze the horn as a receiver of far-field acoustic waves. A comparison of results from each approach is presented in Section III and the range of parameters over which an analytical model is applicable to accurately describe the gain and directivity of an exponential horn receiver are identified. A summary of preliminary results and design applications have been presented previously.[23]

II. METHODS

A. Analytical model

Given a far-field source at angular frequency ω and angle θ relative to the microphone axis, the horn gain is the mean-squared pressure at the horn-loaded microphone, p_h, relative to a free-field microphone, p_f,

$$G(\omega,\theta) = 10\log_{10}\frac{{p_h}^2(\omega,\theta)}{{p_f}^2(\omega,\theta)}. \quad (1)$$

Solving for the gain can be recast into a radiation problem by employing the reciprocity of the wave equation: the pressure at a given point in the far field due to a source at the throat is the same as the pressure that a source at that point in the far field will produce at the throat, assuming everything else equivalent.[24] Therefore, the gain was derived by modeling the radiation from the mouth to the free-field.

A useful approximation for the radiation from the mouth of the horn is the radiation from a spherical cap set in a sphere.[25] The geometry of the spherical cap within a sphere is shown in Fig. 2. The spherical cap is a curved diaphragm set in a rigid sphere of radius a_S and moves with axial velocity u. α is the half-angle of the arc formed by the cap. It has often been assumed that the impedance of the air load upon one side of a vibrating piston in an infinite baffle is a good approximation for the mouth of a horn.[26] The radiation impedance of the spherical cap is similar and there are additional advantages to this model; it captures the wavelength dependent transition from whole-space to half-space radiation and provides the far field pressure in any direction, including behind the radiating surface. Using the boundary value method, the far field pressure is

$$p(r,\theta) = -ik\rho cS\frac{u}{4\pi r}D(\theta), \quad (2)$$

where i is the imaginary unit, k is the wavenumber, ρ is the density of air, c is the speed of sound, S is the dome effective area of the cap, and $D(\theta)$ is the directivity function.[27] The horn serves to alter S and u relative to the free field microphone.

The exact analysis of a radiating horn is severely limited by its complexity, and rigorous analytical solutions do not exist for horns of finite length.[28] Through a series of simplifications,[29] Webster's horn equation can be derived: a one-

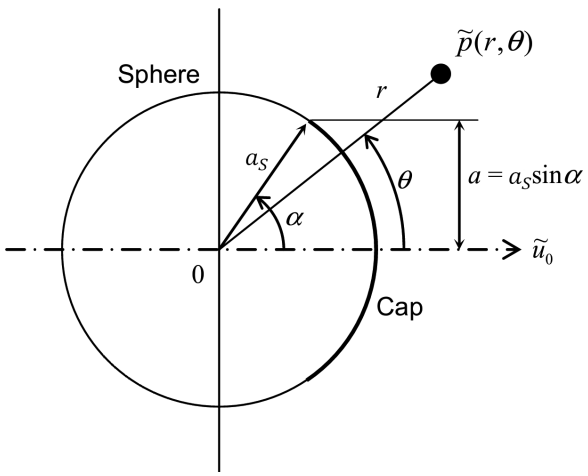

FIG. 2. Geometry of the spherical cap set within a rigid sphere radiation model (adapted from Ref. 27).

dimensional approximation that describes the axial wave motion inside a rigid duct of continuously varying cross sectional area. The primary assumption is that the pressure over any plane perpendicular to the horn axis is uniform in both amplitude and phase, inside and outside the horn. A useful way to write the equation is

$$\frac{\partial^2\phi}{\partial x^2}+\frac{\partial}{\partial x}\ln S\frac{\partial\phi}{\partial x}-\frac{1}{c^2}\frac{\partial^2\phi}{\partial t^2}=0, \tag{3}$$

where ϕ is the velocity potential and S is the cross sectional area at a point x along the axis of the horn.[17] Analytical solutions to Webster's horn equation exist for only a few shapes with consistent change in area along the horn length.[28] Herein, we focus on horns with an exponential flare rate only. The acoustical impedance rapidly reaches unity at a lower frequency than conical or parabolic shapes, resulting in more gain over a wider bandwidth for horns of otherwise similar size.[19,26]

Consider a finite exponential horn with throat at $x=0$, mouth at $x=L$, flare rate m, and cross sectional area $S=S_0e^{mx}$ as shown in Fig. 3. Assume an axisymmetric horn with circular cross section and radius a. Subscripts 0 and L identify quantities at the throat and mouth, respectively. Solving Eq. (3) yields the following general expressions for pressure and particle velocity in terms of traveling waves A and B:

$$p(x,\omega)=-i\omega\rho e^{-mx/2}(Ae^{-i\beta x}+Be^{i\beta x}), \tag{4}$$

$$u(x,\omega)=e^{-mx/2}\left[(-m/2-i\beta)Ae^{-i\beta x}+(-m/2+i\beta)Be^{i\beta x}\right], \tag{5}$$

where $\beta=\sqrt{k^2-m^2/4}$ and $e^{i\omega t}$ has been removed assuming harmonic time dependence. A dispersive standing wave field will exist within the horn. For $k<m/2$, β is imaginary and the waves within the horn are evanescent and rapidly decay with distance. This transition is the cutoff frequency

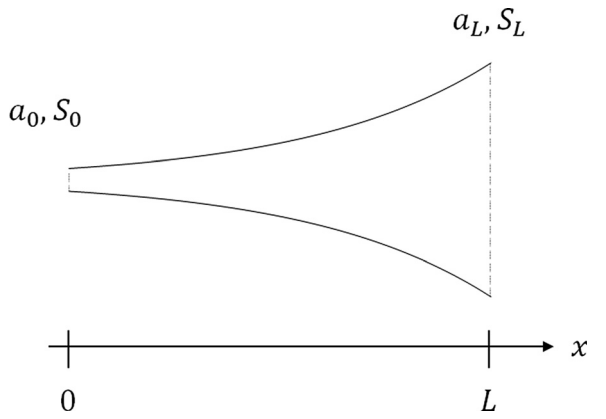

FIG. 3. Geometry of the finite exponential horn.

$$f_c=\frac{mc}{4\pi}. \tag{6}$$

The specific acoustic impedance within the horn can be written in terms of the pressure reflection function, $R=B/A$,

$$z(x,\omega)=-i\omega\rho\frac{e^{-i\beta x}+Re^{i\beta x}}{(-m/2-i\beta)e^{-i\beta x}+(-m/2+i\beta)Re^{i\beta x}}. \tag{7}$$

At $x=L$ the mouth impedance z_m is given by the radiation impedance of the radiating spherical cap. An expression for the reflection coefficient R can be solved for in terms of the impedance at the mouth

$$R_L=\frac{e^{-i\beta L}\left[\frac{z_m}{-i\omega\rho}(-m/2-i\beta)-1\right]}{e^{i\beta L}\left[1+\frac{z_m}{i\omega\rho}(-m/2+i\beta)\right]}. \tag{8}$$

Combining Eqs. (8) and (5) gives an expression for the axial velocity at L,

$$u_L=\frac{u_0\left[(-m/2-i\beta)e^{L(-m/2-i\beta)}+R_L(-m/2+i\beta)e^{L(-m/2+i\beta)}\right]}{-m/2-i\beta+R_L(-m/2+i\beta)}. \tag{9}$$

Finally, Eq. (9) can be substituted into Eq. (2) to yield the far field pressure. The cutoff frequency and frequency dependent response can be specified by manipulating the horn geometry parameters a_0, a_L, and L.

B. Experiment

The substitution method, as specified by IEC 60268-4,[30] was used to measure the frequency-dependent gain of a horn-loaded microphone relative to a free-field microphone. The substitution method is commonly used for calibration and involves placing the system of interest in a known acoustic field as measured by a reference system. Golay complementary sequences[31] were used to obtain the impulse response of the horn-loaded and free-field microphone to an on-axis plane wave.

An axisymmetric exponential horn was fabricated with geometry parameters $a_0=3.7$ mm, $a_L=50.2$ mm, and $L=141$ mm. An electret microphone (Sonion 6297) with 1 mm diameter inlet port was used for both the horn-loaded and free-field reference measurements; the excess space in the horn throat was sealed with clay. Measurements of this horn were made to validate the analytical model in an anechoic chamber in the Electromagnetics Laboratory at Colorado

State University. While this chamber was designed to be anechoic to electromagnetic energy in the radio-frequency range, the absorbent pyramidal cone panels that cover the walls, ceiling, and floor of the chamber also attenuate acoustic energy. The suitability of the chamber for acoustic measurements was evaluated per IEC 60268-4[30] and free field conditions were found to exist above 400 Hz.

C. Numerical model

Because analytical solutions are rarely available, the solution of most scattering problems requires a numerical method. The equivalent source method (ESM) is an inverse method that allows for the calculation of the radiation and scattering from objects in a free-field at a reduced computational load relative to the boundary element method.[32] This is achieved by enclosing an array of "equivalent sources" within the surface and computing the source strengths necessary such that the superposition of acoustic fields satisfies the specified boundary conditions. The boundary conditions are often specified in terms of the acoustic particle velocity on the surface of the object.

Given a far-field source at angle θ, the scattered field of a horn embedded in a rigid sphere was calculated using a matrix formulation of the ESM.[33] The spherical housing is in accordance with the analytical model and also results in a closed system which is more convenient to model. The numerical model was executed in the MATLAB computing environment. Practically, four surfaces were defined: the spherical housing, horn wall, throat, and chamfer. A thin chamfer was added to the interface between the horn mouth and spherical housing to avoid sharp edges on the boundary surface. A rigid boundary was assumed for all surfaces and monopole sources were used for both the incident field and equivalent sources. Figure 4 is a schematic showing the configuration for the equivalent source method using N equivalent sources placed within the boundary jointly defined by the position and normal vectors of M evaluation positions.

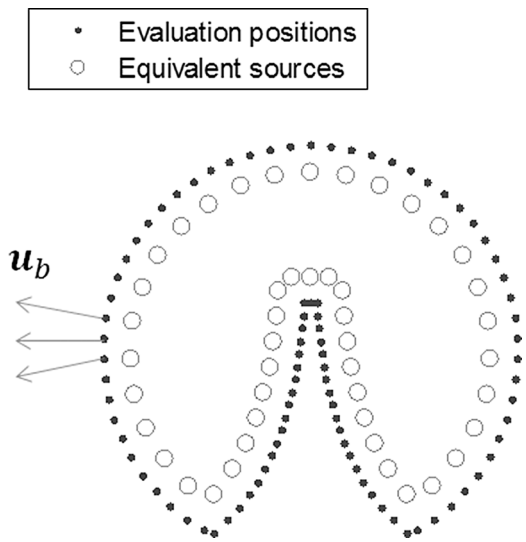

FIG. 4. Two-dimensional schematic showing the configuration of equivalent sources, evaluation positions, and examples of normal vectors, $\boldsymbol{u}_b$, for the three-dimensional numerical model of a horn in spherical housing.

$\boldsymbol{u}_b$ is an $M \times 1$ vector of total normal particle velocities at the boundary due to contributions from the far-field source, $\boldsymbol{u}_{bf}$, and the equivalent sources, $\boldsymbol{u}_{bq}$,

$$\boldsymbol{u}_b = \boldsymbol{u}_{bf} + \boldsymbol{u}_{bq} = \boldsymbol{u}_{bf} + \boldsymbol{T}_e \boldsymbol{q}_e, \tag{10}$$

where $\boldsymbol{T}_e$ is a $M \times N$ matrix that relates the contribution to the normal particle velocities at the boundary from the equivalent sources to the equivalent source strengths, $\boldsymbol{q}_e$. Given the rigid boundary condition, the equivalent sources are driven to produce normal velocities $\boldsymbol{u}_b = 0$ at the evaluation positions. The solution to a fully determined system will exactly satisfy the conditions at the evaluation positions at the expense of points in between. Instead, the normal velocity at the boundary is evaluated at a larger number of evaluation positions that there are equivalent sources.

The ESM error is defined as the residual velocity

$$E = \frac{\boldsymbol{u}_b^H \boldsymbol{u}_b}{\boldsymbol{u}_{bf}^H \boldsymbol{u}_{bf}}. \tag{11}$$

The net velocity squared at the evaluation points is normalized by the velocity squared due to the far field source such that the error ranges from 0 (zero velocity, indicating convergence of the method) to 1 (no equivalent sources operating).

The optimal equivalent source strengths minimize this error in the least squares sense. Because $\boldsymbol{T}_e$ is rectangular, the Moore–Penrose pseudoinverse is calculated to solve for the equivalent source strengths

$$\boldsymbol{q}_e = -\left[\boldsymbol{T}_e^H \boldsymbol{T}_e + \gamma \boldsymbol{I}\right]^{-1} \boldsymbol{T}_e^H \boldsymbol{u}_{bf}, \tag{12}$$

where H denotes the conjugate transpose and $\boldsymbol{I}$ is an $M \times M$ identity matrix. Practically, a regularization term γ is introduced to improve the condition of the matrix prior to inversion. Regularization by a weighting parameter provides a robust solution with minimal increase in the boundary condition error.[34]

The acoustic pressure of the scattered field is calculated at discrete observation points as the superposition of the incident field, $\boldsymbol{p}_{of}$, and equivalent source field

$$\boldsymbol{p}_o = \boldsymbol{p}_{of} + \boldsymbol{p}_{oe} \boldsymbol{q}_e. \tag{13}$$

III. RESULTS

A. Comparison of analytical model and experiment

Considering an on-axis far-field source and the example horn described in Sec. II B, the horn gain was calculated per Eq. (1) for experimental measurement and the analytical model. A comparison of the gain as a function of frequency is shown in Fig. 5. For the analytical gain, radiation from a spherical cap set in a sphere was also used to model the free-field microphone pressure, p_f. Although the simple geometry of this radiation model differs from that of the microphone, at the wavelengths considered the effect of the sphere will be similar to that of any other object of about the same size.[24]

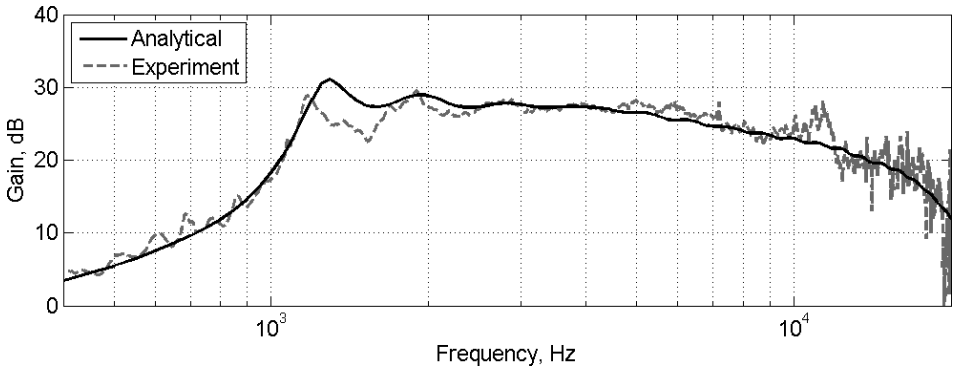

FIG. 5. Comparison of horn gain for an on-axis source as calculated by the analytical model and measured by experiment. The horn exemplified has parameters $a_0 = 3.7$ mm, $a_L = 50.2$ mm, and $L = 141$ mm.

Cap angle $\alpha = 30°$ as suggested by Morse[24] was found to provide a good fit with measurement.

The horn measured has a cutoff frequency of 1 kHz [Eq. (6)]. At frequencies below cutoff, the response changes rapidly with frequency and reactive behavior is dominant.[21] Above cutoff, the horn velocity is relatively constant; the drop in gain at high frequencies, especially above 10 kHz, is due to the radiation model. p_h rolls off above $ka_L = 5$ as the radiation impedance becomes mainly resistive.[27] Meanwhile, as the wavelength becomes comparable to $2\pi a_0$, p_f increases due to the transition from whole-space to half-space radiation. Overall, the gain calculated by the analytical model and experiment match well for this example despite the simplifications of the analytical solution. In addition to the assumptions described in Sec. II A, damping was not accounted for. Noise in the experiment (e.g., imprecise alignment of the on-axis source and receiver, ambient noise) may have also contributed to differences between the analytical and experimental gains.

B. Comparison of analytical and numerical models

The equivalent source method was applied to model the exponential horn embedded in a spherical housing with incident field due to a far field source at angle θ from the horn axis. As with the analytical and experimental approaches, the horn gain of the numerical model was calculated per Eq. (1). An observation point at the center of the throat surface was used to obtain p_h. p_f can be calculated analytically or by a separate ESM model with equivalent results for all practical purposes.

Given the physics of acoustic radiation, the directivity of a horn receiver was expected to be dependent on mouth size; the size of the spherical housing and cap angle may also have some effect. In previous studies, the directivity of horn transmitters has been shown to be related to flare rate when the wavelength is small.[26] To investigate the influence of free design parameters, multiple geometries were modeled with various perturbations of the parameters. In total, seven shapes were considered; independent and derived parameters are shown in Table I. The number of shapes is limited by the burden of constructing accurate numerical models. Horn shape 1 is exemplified in the following two sections to illustrate the gain and directivity as a function of frequency.

TABLE I. Geometrical and acoustical parameters of the horns considered.

Shape	a_0 (mm)	a_L (mm)	L (mm)	m (m^{-1})	f_c (Hz)	a_S (mm)	α (deg)
1	0.5	15.2	65.1	105.0	2866	65.1	13.5
2	0.5	22.9	109.2	70.0	1911	97.6	13.5
3	0.5	7.6	25.9	210.0	5732	32.5	13.5
4	0.5	15.2	17.4	393.7	10746	25	27.9
5	0.5	7.6	18.0	301.8	8383	16.3	27.9
6	0.5	30.5	108.9	75.5	2060	97.6	18.2
7	0.5	38.1	143.6	60.4	1648	97.6	23.0

1. On-axis gain

A plot of the evaluation positions for horn 1 is shown in Fig. 6. Given computational restraints, the number of evaluation positions and equivalent sources in the numerical models is limited. The spacing of evaluation positions must be small relative to a wavelength to well approximate a continuous system. Unfortunately, there is no single best way to position these two elements or determine the minimum number required, although a variety of methods have been explored.[35] For this work, the number and location of evaluation positions and equivalent sources were chosen intuitively and sufficient convergence of the model was evaluated

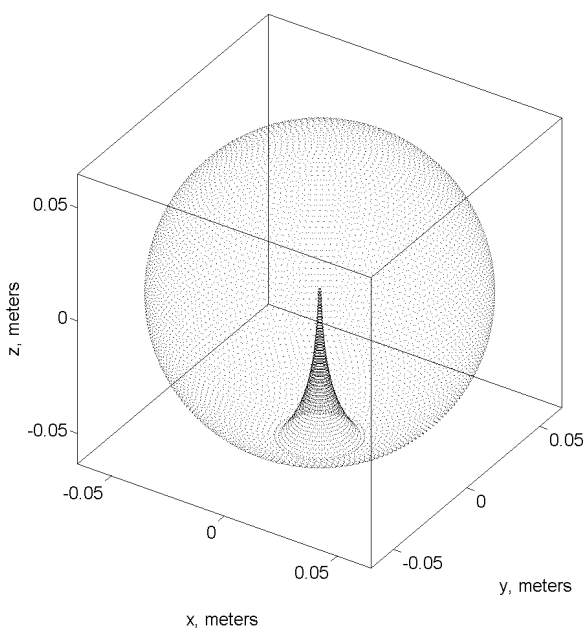

FIG. 6. Evaluation positions (M = 14 337) defining the boundaries of horn shape 1.

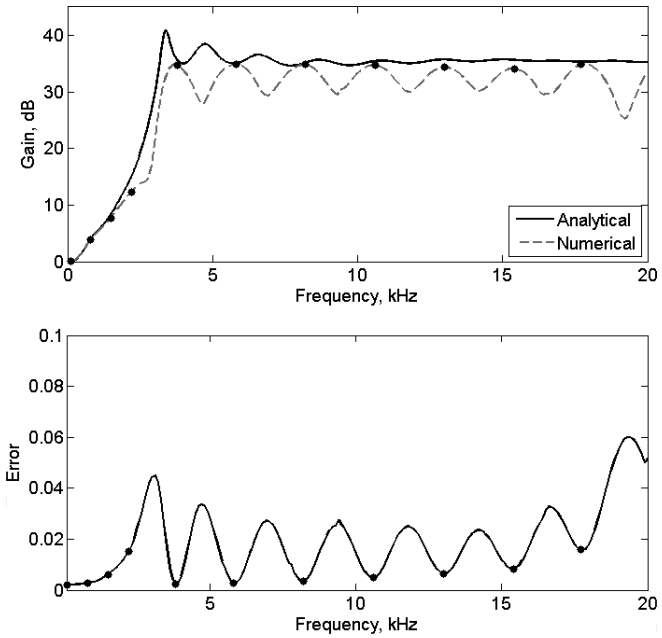

FIG. 7. On-axis gain as given by the analytical and numerical models (top panel) and error of the numerical model (bottom panel) for horn shape 1. Further analysis is limited to the discrete off-resonance frequencies with low error indicated by points.

by the residual velocity error. The error of the numerical model for horn shape 1 appears in Fig. 7. One trend is a gradual increase in error with frequency as the wavelength becomes smaller compared to the discretized boundary. The cyclical trend is related to the horn gain and resonance in particular.

The gains of both the analytical and numerical models of horn shape 1 are shown in Fig. 7 for comparison. Although the error is very low across the entire frequency range, gain is sensitive to error. The horn has multiple resonant frequencies. Not a completely closed system, the response is finite at resonant frequencies. Still, it is difficult for the equivalent sources to satisfy the boundary conditions at resonance and the error is higher at these frequencies. Incorporating damping may alleviate, but damping was difficult to replicate across the analytical, experimental, and numerical analyses and not applied. The numerical and analytical models match well at discrete frequencies where E is low and further analysis of the numerical models is limited to these off-resonance frequencies (points in Fig. 7).

The frequency-domain solution of the equivalent source method is the steady-state scattered pressure. Figure 8 shows the spatially varying phase of the pressure at a frequency of 10.6 kHz ($ka_L = \pi$) and 17.7 kHz ($ka_L = 5$). The steady-state response is a summation of the incident and scattered energy and the expanding surface area produces a curvature in the resulting wavefronts (each isophase surface). Spherical cap-like wavefronts have been experimentally measured[21,29] and are in accordance with the assumed radiation model of the analytical solution.

The assumption of planar wavefronts inherent to Webster's equations is only satisfied if the diameter is small compared to wavelengths. Indeed, for $ka_L > \pi$ the phase response indicates the presence of higher order modes (Fig. 8). The energy of higher order modes comes at the expense of the fundamental mode. However, the gain calculated from numerical models at high frequencies is not significantly different from the analytical solution, which only accounts for the fundamental mode. While an incident plane wave will excite higher order modes within the horn, these propagate towards the throat until the decreasing diameter raises the cutoff frequency and energy rejoins the fundamental mode. Similar behavior is also observed in the other shapes in Table I and demonstrates that the 1-D approximation can provide accurate estimates of gain at high frequencies for waves incident on-axis.

2. Off-axis gain

The response of horn shape 1 was analyzed as a function of angle at discrete frequencies with low ESM error. Given the geometrical symmetry, the analysis can be curtailed to angles from 0° to 180° in one plane only. ESM error varied slightly with source angle although the relationships with wavelength and resonance described above are dominant (not shown). Directivity patterns of horn shape 1 appear in Fig. 9 and show the gain relative to an on-axis source at

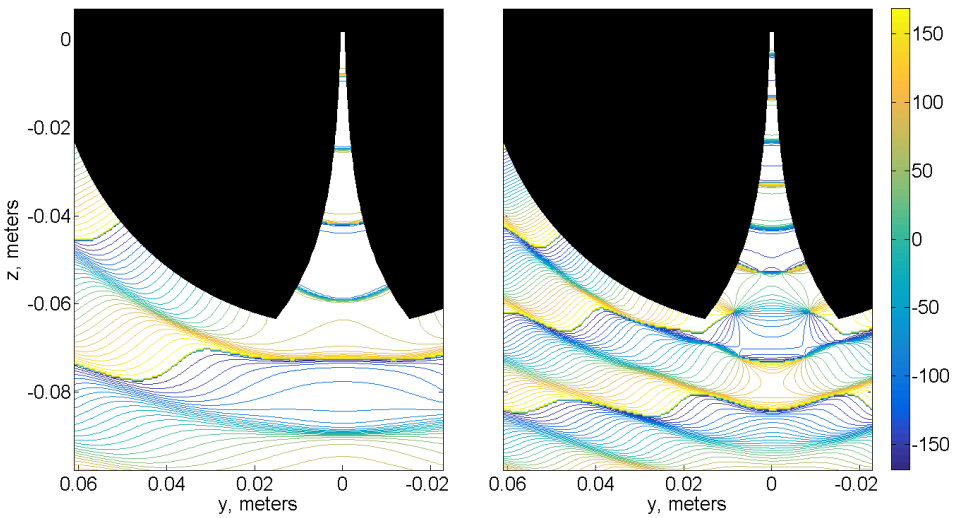

FIG. 8. (Color online) Phase contours of the scattered pressure (degrees) for horn shape 1 in response to an on-axis source at 10.6 kHz (left panel) and 17.7 kHz (right panel).

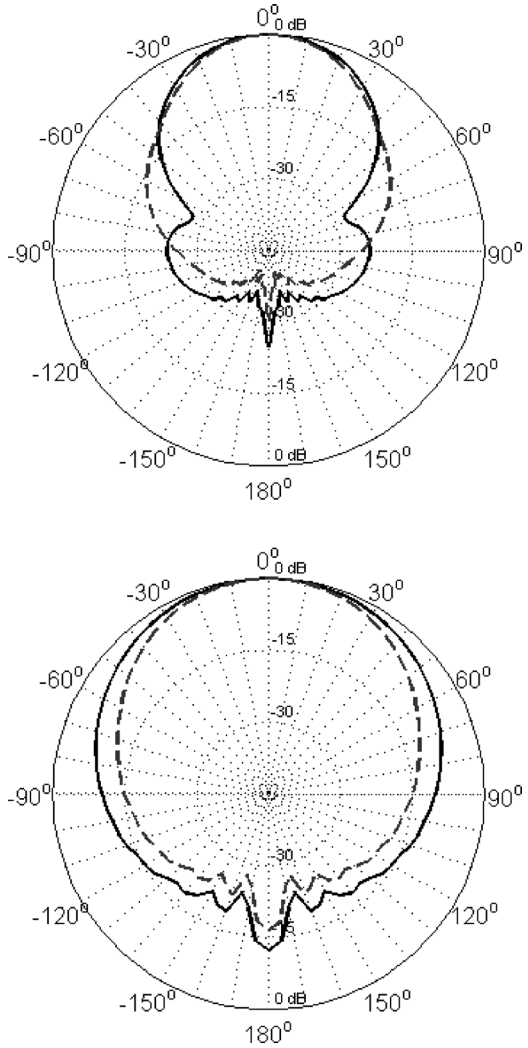

FIG. 9. Horn shape 1 directivity patterns from the analytical (—) and numerical (--) models at 8.2 kHz (bottom panel) and 15.4 kHz (top panel).

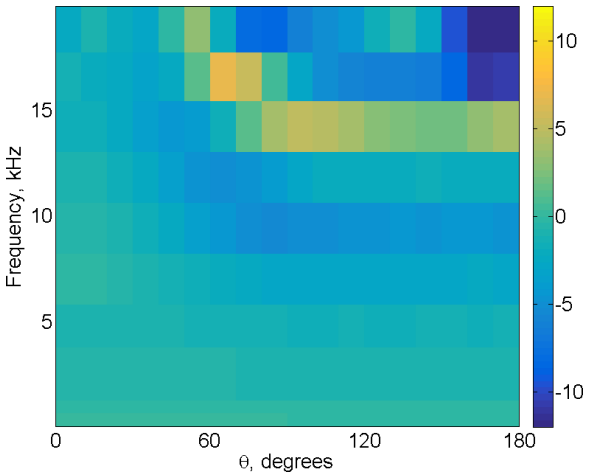

FIG. 10. (Color online) Surface plot showing the difference (dB) between the directivity patterns calculated by the analytical and numerical models for horn shape 1.

8.2 kHz ($ka_L = 2.3$) and 15.4 kHz ($ka_L = 4.3$). The patterns described by the analytical and numerical models agree on-axis and at low frequencies. There is less agreement off-axis; often the analytical model overestimates gain although there are exceptions at some frequencies and angles. Notating the gain of the analytical and numerical model as G_a and G_n, respectively, the differences are summarized in a surface plot of $\Delta G = G_n - G_a$ (Fig. 10). The region of agreement at small angles and low frequencies is clear in Fig. 10; behavior consistent with angle of incidence is also apparent.

The mechanism responsible for reduced gain can be induced from plots of the phase of the scattered pressure, see Fig. 11. Waves incident from off-axis diffract around the housing and propagate into the horn mouth. Inside the horn, the walls compel approximately planar wavefronts near the throat. At the mouth, plots of the phase response reveal a zone of complex behavior where energy diffracts into the horn. In this space, wavefronts are not aligned with the horn axis and therefore do not concentrate energy towards the throat, resulting in less gain for waves arriving off-axis. To a first order approximation, the horn gain is the ratio of the mouth to throat area: $G \approx 10\log_{10}(S_L/S_0)$. The presence of the diffraction zone results in a horn with a smaller effective mouth area. As the example in Fig. 11 shows, a smaller diffraction zone and less gain reduction can occur at a higher frequency for the same angle of incidence. At very high frequencies the complexity of the diffraction results in behavior that cannot be accounted for by the analytical model.

Consideration of a spherical housing leads to some phenomena idiosyncratic to smooth shapes. The size of the diffraction zone varies non-monotonically with both wavelength and angle of incidence, although it can be fairly similar across angle (Fig. 10). For most angles of incidence, energy must travel around the housing to the mouth. The curvature of the housing dictates the effective angle of incidence, leading to consistent behavior. At some frequencies and angles of incidence, the gain of the numerical model is greater than that of the analytical model (15.4 kHz for example, see Fig. 9). A diffraction zone still reduces the effective mouth size, but more significantly the analytical model is based on a uniform spherical housing which experiences strong deconstructive interference for some combinations of path length and wavelength. The numerical model accounts for the presence of the horn cavity which disrupts the symmetry by forcing a diversity of path lengths with varying phase.

3. Geometrical parameters and applicability of the analytical model

Design of horn receivers can benefit from a rule of thumb that summarizes the limitations of an analytical model given horn geometry. The suite of horns described in Table I was analyzed similarly to shape 1. Gain as a function of angle was calculated by the analytical and numerical models at discrete frequencies with low ESM error. In a broad sense, all of the horns exhibit similar behavior in that there is strong agreement between the models at low frequencies and angles. The scattering behavior described in Sec. III B 2 is also present and yields a region of varying disagreement at high frequencies as shown in Fig. 10. The regions can be delineated by a critical frequency, defined as the frequency

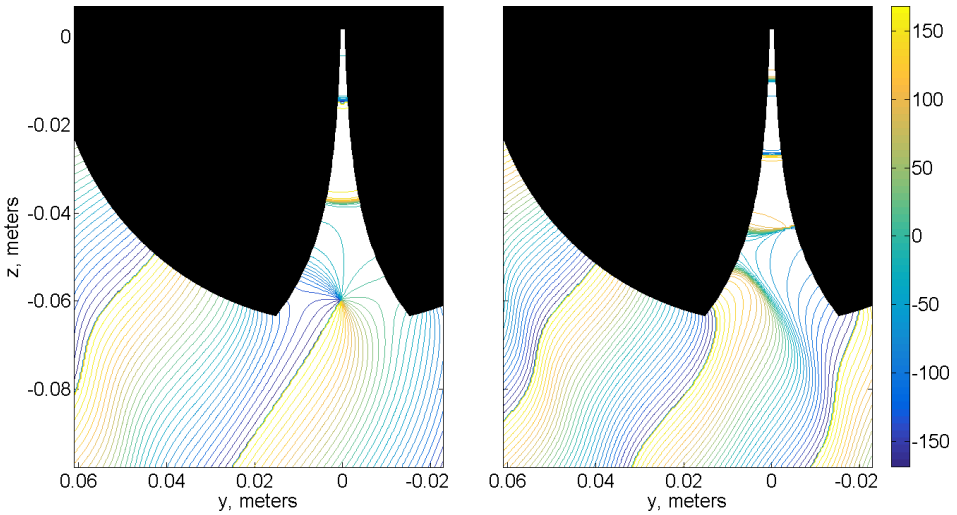

FIG. 11. (Color online) Phase contours of the scattered pressure (degrees) for horn shape 1 in response to a source incident at $\theta = 120°$. A source frequency of 8.2 kHz (left panel) results in a larger diffraction zone and less gain than a source frequency of 10.6 kHz (right panel).

at which $\Delta G < 3$ dB. The angle at which the critical frequency is evaluated is somewhat arbitrary given the consistency of behavior with this parameter off-axis. The critical frequency was calculated for the horns in Table I at an angle of incidence $\theta = 90°$.

Despite the coarse frequency resolution of the numerical solutions, there is a strong relationship between the critical frequency and mouth sizes across horns with diverse geometries. Figure 12 is a scatterplot of the wavelength at the critical frequency, λ_c, versus $4a_L$. From this plot, it can be induced that the analytical model well approximates the directivity of the horn receivers for $ka_L < \pi/2$. This limit of applicability is similar to the general assumption for Webster's horn equation ($ka_L \ll \pi$). No significant relationships with other parameters were apparent, likely a consequence of the small sample size.

The directivity index[23] was also calculated for all shapes. The difference in the directivity index calculated by the numerical and analytical models generally increases with frequency, but did not exceed 3 dB for any of the shapes ($ka_L \approx 11$ was the largest considered). Because the directivity index essentially averages across angles, it is a less precise indicator. However, this suggests even greater applicability for the use of an analytical model to describe the horn response in a diffuse field.

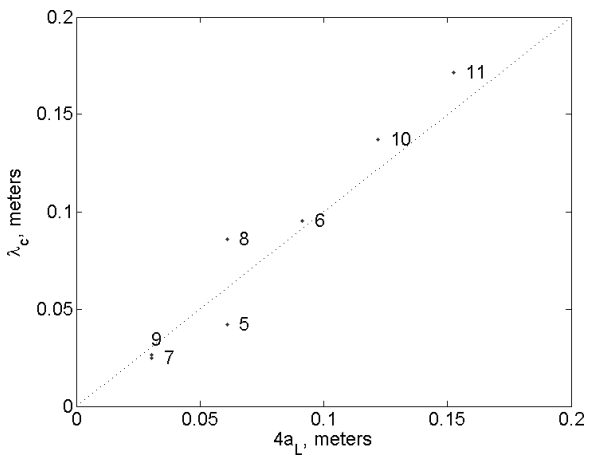

FIG. 12. Scatter plot showing the relationship between mouth radius, a_L, and critical wavelength, λ_c, for the horn shapes in Table I.

IV. CONCLUSIONS

The gain and directivity of the exponential horn receiver is a spherical enclosure has been analyzed using analytical, numerical, and experimental methods. The horn receiver offers substantial advantages for acoustic monitoring applications requiring high sensitivity and control of directivity. Using available microphones, horn receivers can be constructed to achieve an effective noise floor that allows for focused measurement of very quiet sounds and environmental monitoring in quiet areas. Shadowing and the exaggerated relationship between phase and angle of incidence due to diffraction also suggest that an array of horn receivers can enhance beamforming performance relative to omnidirectional sensors.

The analytical model, based on Webster's horn equation and radiation from a spherical cap, provides a way to rapidly assess the gain and directivity across frequency given geometrical parameters. The analytical model was validated by experimental measurement. Although the one-dimensional approximation neglects to account for higher order modes, this approach provides an accurate model for waves incident on-axis over a greater range of frequencies than anticipated. The relative simplicity of the analytical model makes it useful for design applications. However, precise knowledge of directivity is critical in the design of receivers for environmental sound monitoring requiring calibrated measurements.

A comprehensive analysis of receiver directivity required a numerical method that can account for complex acoustic scattering. The three-dimensional equivalent source model was applied to an exponential horn embedded in a rigid spherical housing to describe higher order modes, diffraction, and shadowing. Analyses of the phase of the scattered pressure revealed that gain is often overestimated by the analytical model for an off-axis source. The numerical model revealed the presence of a diffraction zone at the horn mouth in which wavefronts are not aligned with the horn axis, resulting in less gain from an effectively smaller horn. Consideration of multiple horns of varying geometry showed

that the analytical and numerical models were in agreement at low frequencies and small angles of arrival. Off-axis, the analytical model provides accurate estimates of gain for $ka_L < \pi/2$. The sample size of receiver shapes was not adequate to discern an effect of other free design parameters. The analysis was limited to exponential horns whereas other area profiles may result in more desirable directional characteristics. The numerical analysis was also limited to discrete frequencies off resonance. However, the behavior described in Sec. III B 2 showed that diffraction effectively results in a horn of shorter length which suggests that the frequencies of resonance may shift for waves arriving off-axis. At frequencies near resonance, the analytical model is expected to have reduced ability to describe the true response.

Because the gain of horns is proportional to the ratio of mouth to throat size, horns can provide substantial gain at wavelengths larger than the horn. The small size of micro-electro-mechanical microphones makes this achievable in the audible frequency range, although designs must make a tradeoff between gain and directivity. Theoretically, performance will increase as even smaller diaphragm microphones become available. Practical realization of such horn-loaded devices is limited by the ability to accurately fabricate horns with very small orifices and future research should also consider the role of thermoviscous losses.

ACKNOWLEDGMENTS

This work was funded by the United States National Park Service.

[1]D. T. Blumstein, D. J. Mennill, P. Clemins, L. Girod, K. Yao, G. Patricelli, J. L. Deppe, A. H. Krakauer, C. Clark, K. A. Cortopassi, and S. F. Hanser, "Acoustic monitoring in terrestrial environments using microphone arrays: Applications, technological considerations, and prospectus," J. Appl. Ecol. **48**, 758–767 (2011).
[2]M. Campos Cerqueira and M. T. Aide, "Improving distribution data of threatened species by combining acoustic monitoring and occupancy modeling," Methods Ecol. Evol. **7**, 1340–1348 (2016).
[3]M. E. Thompson, S. J. Schwager, and K. B. Payne, "Heard but not seen: An acoustic survey of the African forest elephant population at Kakum Conservation Area, Ghana," Afr. J. Ecol. **48**, 224–231 (2010).
[4]T. A. Marques, L. Thomas, S. W. Martin, D. K. Mellinger, J. A. Ward, D. J. Moretti, D. Harris, and P. L. Tyack, "Estimating animal population density using passive acoustics," Biol. Rev. Cambridge Philos. Soc. **88**, 287–309 (2013).
[5]D. J. Mennitt and K. M. Fristrup, "Influence factors and spatiotemporal patterns of environmental sound levels in the contiguous United States," Noise Control Eng. J. **64**, 342–353 (2016).
[6]E. Lynch, D. Joyce, and K. Fristrup, "An assessment of noise audibility and sound levels in U.S. National Parks," Landsc. Ecol. **26**, 1297–1309 (2011).
[7]L. Fritschi, L. Brown, R. Kim, D. Schwela, and S. Kephalopolous, *Burden of Disease from Environmental Noise: Quantification of Healthy Life Years lost in Europe* (World Health Organization, Bonn, 2011).
[8]G. Shannon, M. F. McKenna, L. M. Angeloni, K. R. Crooks, K. M. Fristrup, E. Brown, K. A. Warner, M. D. Nelson, C. White, J. Briggs, and S. McFarland, "A synthesis of two decades of research documenting the effects of noise on wildlife," Biol. Rev. **91**, 982–1005 (2015).
[9]B. C. Pijanowski, A. Farina, S. H. Gage, S. L. Dumyahn, and B. L. Krause, "What is soundscape ecology? An introduction and overview of an emerging new science," Landsc. Ecol. **26**, 1213–1232 (2011).
[10]R. Horonjeff, "Overcoming instrument noise when measuring in quiet environments," in *Proceedings of Inter-noise* (2002).
[11]D. J. Mennitt, K. Fristrup, and K. Sherrill, "A geospatial model of ambient sound pressure levels in the contiguous United States," J. Acoust. Soc. Am. **135**, 2746–2764 (2014).
[12]E. Lynch, L. M. Angeloni, K. Fristrup, D. Joyce, and G. Wittemyer, "The use of on-animal acoustical recording devices for studying animal behavior," J. Ecol. Evol. **3**, 2030–2037 (2013).
[13]H. R. Goerlitz, S. Greif, and B. M. Siemers, "Cues for acoustic detection of prey: Insect rustling sounds and the influence of walking substrate," J. Exp. Biol. **211**. 2799–2806 (2008).
[14]R. Fay, *Hearing in Vertebrates: A Psychophysics Databook* (Hill-Fay Associates, Winnetka, IL, 1988).
[15]S. Wahlström, "The parabolic reflector as an acoustical amplifier," J. Aud. Eng. Soc. **33**, 418–429 (1985).
[16]N. H. Fletcher, "Acoustic systems in biology: From insects to elephants," Acoust. Austr. **33**, 83–88 (2005).
[17]H. F. Olson and I. Wolff, "Sound concentrator for microphones" J. Acoust. Soc. Am. **1**, 410–417 (1930).
[18]D. M. Donskoy and B. A. Cray, "Acoustic particle velocity horns," J. Acoust. Soc. Am. **131**, 3883–3890 (2012).
[19]K. M. Fristrup and D. Mennitt, "Bioacoustical monitoring in terrestrial environments," Acoust. Today **8**, 16–24 (2012).
[20]E. Eisner, "Complete solutions of the 'Webster' horn equation," J. Acoust. Soc. Am. **41**, 1126–1146 (1967).
[21]K. R. Holland, F. J. Fahy, and C. L. Morfey, "Prediction and measurement of the one-parameter behavior of horns," J. Aud. Eng. Soc. **39**, 315–337 (1991).
[22]M. R. Stinson and G. A. Daigle, "Comparison of an analytic horn equation approach and a boundary element method for the calculation of sound fields in the human ear canal," J. Acoust. Soc. Am. **118**, 2405–2411 (2005).
[23]D. J. Mennitt and K. Fristrup, "Gain and directivity of exponential horn receivers," J. Acoust. Soc. Am. **140**, 3140 (2016).
[24]P. M. Morse, *Vibration and Sound* (Acoustical Society of America, New York, 1981).
[25]T. F. Johansen, "On the directivity of horn loudspeakers," J. Aud. Eng. Soc. **42**, 1008–1019 (1994).
[26]H. F. Olson, *Elements of Acoustical Engineering* (D. Van Nostrand Company, New York, 1947).
[27]L. Beranek and T. Mellow, *Acoustics: Sound Fields and Transducers* (Academic Press, New York, 2012).
[28]V. Salmon, "Horns," in *Encyclopedia of Acoustics*, edited by M. J. Crocker (John Wiley, New York, 1997), Vol. 4, pp. 1925–1931.
[29]W. M. Hall, "Comments on the Theory of Horns," J. Acoust. Soc. Am. **3**, 552–561 (1932).
[30]IEC Standard 60268-4: *Sound System Equipment Part 4: Microphones* (International Electrotechnical Commission, Geneva, Switzerland, 2004).
[31]B. Zhou and D. Green, "Characterization of external ear impulse responses using Golay codes," J. Acoust. Soc. Am. **92**, 1169–1171 (1992).
[32]G. H. Koopmann, L. Song, and J. B. Fahnline, "A method for computing acoustic fields based on the principle of wave superposition," J. Acoust. Soc. Am. **86**, 2433–2438 (1989).
[33]M. Johnson, S. Elliott, K. Baek, and J. Garcia-Bonito, "An equivalent source technique for calculating the sound field inside an enclosure containing scattering objects," J. Acoust. Soc. Am. **104**, 1221–1231 (1998).
[34]B. Lam, S. J. Elliott, J. Cheer, and W. Gan, "Regularisation of the equivalent source method for robust numerical modelling of acoustic scattering," in *Proceedings of Inter-Noise* (2015).
[35]Y. J. R. Gounot and R. E. Musafir, "Simulation of scattered fields: Some guidelines for the equivalent source method," J. Sound Vib. **330**, 3698–3709 (2011).